

Metadata of the article that will be visualized in OnlineFirst

ArticleTitle	Assessment of the durability of various cementitious materials subjected to low levels of H ₂ S in wastewater networks	
--------------	-----------------------------------------------------------------------------------------------------------------------------------	--

Article Sub-Title		
-------------------	--	--

Article CopyRight	The Author(s), under exclusive licence to RILEM (This will be the copyright line in the final PDF)	
-------------------	-------------------------------------------------------------------------------------------------------	--

Journal Name	Materials and Structures	
--------------	--------------------------	--

Corresponding Author	FamilyName	Ayoub
	Particle	
	Given Name	Janette
	Suffix	
	Division	MAST-CPDM
	Organization	University Gustave Eiffel
	Address	Mame-La-Vallée, 77454, Paris, France
	Phone	
	Fax	
	Email	janette.ayoub@univ-eiffel.fr
URL		
ORCID	http://orcid.org/0009-0005-4045-6058	

Author	FamilyName	Minerbe
	Particle	
	Given Name	Marielle Guéguen
	Suffix	
	Division	MAST-CPDM
	Organization	University Gustave Eiffel
	Address	Mame-La-Vallée, 77454, Paris, France
	Phone	
	Fax	
	Email	marielle.gueguen@univ-eiffel.fr
URL		
ORCID		

Author	FamilyName	Pons
	Particle	
	Given Name	Tony
	Suffix	
	Division	MAST-CPDM
	Organization	University Gustave Eiffel
	Address	Mame-La-Vallée, 77454, Paris, France
	Phone	
	Fax	
	Email	tony.pons@univ-eiffel.fr
URL		
ORCID		

Author	FamilyName	Oliveira
	Particle	
	Given Name	Marcos
	Suffix	
	Division	
	Organization	SIAAP- Direction Innovation
	Address	82 Avenue Kléber, 92700, Colombes, France
	Phone	
	Fax	
	Email	marcos.oliveira@siaap.fr
URL		
ORCID		

Author	FamilyName Particle Given Name Suffix Division Organization Address Phone Fax Email URL ORCID	Guérin-Rechdaoui Sabrina SIAAP- Direction Innovation 82 Avenue Kléber, 92700, Colombes, France sabrina.guerin@siaap.fr
Author	FamilyName Particle Given Name Suffix Division Organization Address Phone Fax Email URL ORCID	Marchetti Mario MAST-UMR MCD University Gustave Eiffel-Cerema Mame-La-Vallée, 77454, Paris, France mario.marchetti@univ-eiffel.fr
Schedule	Received Revised Accepted	8 Dec 2023 28 Mar 2024
Abstract	Wastewater networks are intrinsically attacked by the production of H ₂ S, a highly reactive gas known for its extremely aggressive nature. This study employs a range of techniques, such as XRD, SEM–EDS, TGA, and Raman spectrometry, to investigate the interaction between low concentrations of H ₂ S—averaging 1.3 ppm and various types of Portland cementitious materials (CEM I, CEM II, CEM III, and CEM V). The objective is to discern the chemical alterations contributing to structural deterioration and to provide a mineralogical characterization of the deterioration layers present on these binders.	
Keywords (separated by '-')	Biodeterioration - Cementitious materials - Low H ₂ S concentration - Durability - SEM–EDS - μ-Raman	
Footnote Information		



2 Assessment of the durability of various cementitious 3 materials subjected to low levels of H₂S in wastewater 4 networks

5 Janette Ayoub · Marielle Guéguen Minerbe ·
6 Tony Pons · Marcos Oliveira ·
7 Sabrina Guérin-Rechdaoui · Mario Marchetti

8 Received: 8 December 2023 / Accepted: 28 March 2024
9 © The Author(s), under exclusive licence to RILEM 2024

10 **Abstract** Wastewater networks are intrinsically
11 attacked by the production of H₂S, a highly reactive
12 gas known for its extremely aggressive nature. This
13 study employs a range of techniques, such as XRD,
14 SEM–EDS, TGA, and Raman spectrometry, to investi-
15 gate the interaction between low concentrations of
16 H₂S—averaging 1.3 ppm and various types of Port-
17 land cementitious materials (CEM I, CEM II, CEM
18 III, and CEM V). The objective is to discern the
19 chemical alterations contributing to structural deterio-
20 ration and to provide a mineralogical characterization
21 of the deterioration layers present on these binders.

Through a comprehensive examination of the durabil-
ity of these materials exposed to low concentrations
of H₂S in a Paris Region sewage system over nearly
four years, the findings extend beyond surface-level
observations. Despite the absence of visible signs of
deterioration, high-precision analytical techniques
reveal significant mineralogical transformations
within the cementitious matrix. Expansive products
such as gypsum, ettringite, and elemental sulfur are
identified in mortar samples, underscoring the critical
role of precise analysis in comprehending the deterio-
ration process.

Keywords Biodeterioration · Cementitious
materials · Low H₂S concentration · Durability ·
SEM–EDS · μ -Raman

1 Introduction

Underneath the dynamic urban landscape lies a com-
plex and often overlooked sewer system network that
silently plays a crucial part in ensuring public health
and environmental sustainability. Cementitious mate-
rials, which form the backbone of the sewer network,
are at the root of the success of these underground
pipes. These materials are a key to ensuring the sewer
infrastructure’s structural integrity, durability, and
overall efficiency.

Indeed, throughout their lifespan, these pipes
encounter a range of deterioration processes, which

A1 J. Ayoub (✉) · M. G. Minerbe · T. Pons
A2 MAST-CPDM, University Gustave Eiffel,
A3 Marne-La-Vallée, 77454 Paris, France
A4 e-mail: janette.ayoub@univ-eiffel.fr

A5 M. G. Minerbe
A6 e-mail: marielle.gueguen@univ-eiffel.fr

A7 T. Pons
A8 e-mail: tony.pons@univ-eiffel.fr

A9 M. Oliveira · S. Guérin-Rechdaoui
A10 SIAAP- Direction Innovation, 82 Avenue Kléber,
A11 92700 Colombes, France
A12 e-mail: marcos.oliveira@siaap.fr

A13 S. Guérin-Rechdaoui
A14 e-mail: sabrina.guerin@siaap.fr

A15 M. Marchetti
A16 MAST-UMR MCD, University Gustave Eiffel-Cerema,
A17 Marne-La-Vallée, 77454 Paris, France
A18 e-mail: mario.marchetti@univ-eiffel.fr



can arise from assembly defects, environmental constraints, or deterioration triggered by the presence of substances and microorganisms within the pipe. Thus, in about 40% of cases, this damage can be linked to a biogenic attack resulting from sulfuric acid production [1]. This particular mode of deterioration, encountered in concrete structures subjected to sewage environments, has the potential to substantially reduce the lifespan of these structures [2, 3]. For instance, it can diminish the 100-year expected service life to a range of 30–50 years, or even, in the most severe cases, to 10 years or less [3, 4].

The phenomenon of microbiologically induced acid deterioration in concrete has garnered significant attention since its identification. The sequence of stages that initiate and advance concrete biodeterioration in sewage environments has been delimited into several steps by various researchers [3, 5–11]. However, the most commonly agreed-upon sequences can be summarized as previously schematized by Herisson et al. [12]. This process begins with the creation of anaerobic zones at the bottom of pipes by wastewater sediments. In these specific zones, the low concentration of oxygen leads sulfate-reducing bacteria (SRB) to reduce sulfur compounds, such as sulfates, into highly volatile hydrogen sulfide (H_2S). Subsequently, depending on the network's temperature, pH, hydrodynamics, and the concentration of oxidized sulfur compounds in the wastewater, H_2S volatilizes into the pipe atmosphere above the water flow. Gaseous H_2S condenses on the pipe surface and affects the cementitious matrix in two distinct yet interconnected ways. The first of these pathways acts directly by reducing the surface pH of cementitious materials, resulting in immediate effects. Nevertheless, it's important to note that, at this stage, the pH cannot attain an acidic value. However, the second, more complex path involves a fascinating chain of four key stages: the initial abiotic conversion of H_2S into sulfur components on the surface of the cementitious material; the subsequent bacterial oxidation of sulfur compounds into sulfuric acid; the diffusion of sulfuric acid into the cementitious matrix; and ultimately the gypsum formation.

The biodeterioration of sewage cementitious matrices has attracted considerable global research attention, with notable studies in occidental countries such as Australia, Austria, France, Germany, Denmark, and the United States among others [6–8, 10,

13]. However, among these studies, the H_2S levels investigated consistently reached high concentrations, which often exceeded 600 ppm, leaving a gap in research into low H_2S concentrations. Consequently, the ability of sewage cementitious materials to withstand low H_2S environmental conditions remains under-explored.

This study addresses this gap by investigating the performance and durability of various Portland cementitious materials (CEM I, CEM II, CEM III, and CEM V) under low H_2S concentrations exposure. Additionally, it provides a mineralogical characterization of deterioration layers found on these binders. Understanding the processes in the cementitious matrix at low H_2S concentrations is crucial for implementing effective prevention and maintenance procedures, ensuring the long-term durability and performance of vital infrastructure in wastewater networks.

Accordingly, different mortar formulations were exposed in situ for a period of nearly 4 years in a sewage system, with periodic macroscopic monitoring. Various analytical techniques found application in this study, such as X-ray diffraction (XRD), scanning electron microscopy equipped with an energy-dispersive X-ray spectrometer (SEM-EDS), and thermogravimetric analysis (TGA). Furthermore, by leveraging this wide range of practical instrument configurations, Raman spectrometry outperforms other methods with its diverse advantages [14, 15]. This technique is nowadays widely applied to characterize civil engineering materials and continuously assess their evolution throughout their life cycle, from initial anhydrous materials to hydrated and hydrating pastes, and all the way to their degraded state [16–18].

2 Materials and experimental approaches

2.1 Mortar samples

These mixtures were established to be representative of the real-world sewer network to assess their resistance to deterioration.

The mortar specimens used in this study were prepared with four different types of cement: ordinary Portland cement (CEM I), Portland-composite cement (CEM II), blast furnace cement (CEM III), and composite cement (CEM V). Three specimens



143 were prepared for each type of cement. In all mix-
 144 tures, the water-to-cement ratio was 0.5 and the sand-
 145 to-cement ratio was 3. The mortars were molded into
 146 cylinders with a 6 cm diameter and a 12 cm height. A
 147 PVC tube was also precisely inserted into the central
 148 portion of each sample to ease their handling.

149 Once formed, the specimens were exposed to a
 150 100% relative humidity atmosphere over 24 h, then
 151 unmolded and stored in sealed plastic bags for a cur-
 152 ing period of 28 days. Then, they were placed inside
 153 a 60×40×30 cm³ compartment that was afterward
 154 installed inside the sewer network and exposed to the
 155 specific sewer gas flow. Figures 1 and 2 in Herisson
 156 et al.'s [12] study provide a clear understanding of the
 157 appearance and placement of the specimens on site.

158 2.2 Exposure site of mortar samples

159 The northern part of the greater Paris Sanitation
 160 Authority (SIAAP in French), has been selected as a
 161 suitable exposure site for the 44 months study period.
 162 In addition to stormwater and industrial wastewater,
 163 SIAAP carries and purifies the wastewater of nine
 164 million residents within and around Paris, enhancing
 165 the dynamic natural environments of the Seine and

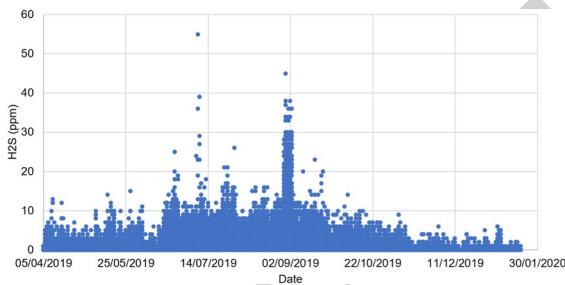
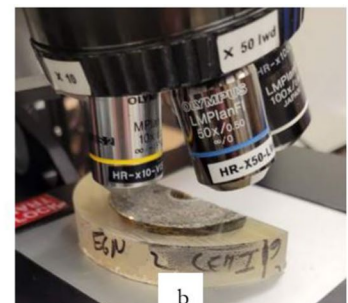


Fig. 1 H₂S concentration versus Time over 9 months at the SIAAP facility

Fig. 2 LabRam HR800 (a) and CEM I sample before 2D mapping (b)



166 Marne rivers. The selected site has been chosen based
 167 on precise previous results showing that the area
 168 exhibited relatively low H₂S concentrations.

169 OdaLog® safety sensors were inserted alongside
 170 the samples in the compartment in order to track the
 171 concentration of H₂S and temperature throughout the
 172 study period. Figure 3 and Table 1 present a 9-month
 173 example of the results obtained from these sensors
 174 used to assess the environmental conditions. During
 175 this period, the site recorded an average H₂S concen-
 176 tration of 1.3 ppm, which categorizes it as a mod-
 177 erately chemically aggressive environment accord-
 178 ing to the NF EN 206/CN [19], designated as XA2.

Cement	T0	21 months	29 months	44 months
CEM I				
CEM II				
CEM III				
CEM V				

Fig. 3 In-situ visual evolution of mortar samples exposed over 44 months at a low H₂S concentration



Table 1 Overview of H₂S concentration (ppm) data over 9 months of the study period

Mean	Standard deviation	1st quartile	3rd quartile	Minimum	Maximum
1.3	2.7	0.0	1.0	0.0	55.0

179 Moreover, as detailed in Table 1, the data shows that
 180 the first quartile stands at 0.0 ppm, representing the
 181 lower 25% of the measured concentrations, while
 182 the third quartile is at 1.0 ppm, signifying the value
 183 below which 75% of the data falls. The computed
 184 values presented in Table 1 provide a comprehensive
 185 view of the distribution of H₂S concentrations, which,
 186 in turn, reveals that the specimens were not exposed
 187 to a severe H₂S environment with respect to this gas.

188 **2.3 Testing procedure**

189 *2.3.1 In-situ evolution monitoring*

190 At each sampling time step (21, 29, and 44 months
 191 after exposure), in situ photographs of the specimens
 192 were captured to document the macroscopic degra-
 193 dation of the specimens over time. Additionally, the
 194 weights of the mortars (measured with a scale accu-
 195 rate to 0.1 g), surface pH (determined using pH paper
 196 with a precision of 0.2), and diameters (measured
 197 with a caliper) were recorded to monitor changes in
 198 the properties over time.

199 After a 44-month exposure period in the sewage
 200 network, the mortars were carefully collected from
 201 their cases and accurately processed to secure consist-
 202 ent test conditions and results. The specimens were
 203 then entirely covered with epoxy resin (EpoFix, Stru-
 204 ers) under vacuum conditions to preserve the deterio-
 205 ration condition. This precaution was taken to ensure
 206 the sample’s structural integrity for further testing.

207 Before all the analysis, the mortars exposed in-situ
 208 for 44 months underwent a meticulous diamond pol-
 209 ishing process with ethanol that yielded homogene-
 210 ous and plane test surfaces.

211 *2.3.2 Scanning electron microscopy with energy
 212 dispersive x-ray spectrometer (SEM–EDS)*

213 Analyses were carried out using a Scanning elec-
 214 tron Microscope (Quanta 400 FEI) equipped with

an Energy Dispersive X-ray Spectrometer (EDS, Xplore30, Oxford), operating at an acceleration volt- age of 20 kV. After carbon metallization of the pol- ished surface, a panorama was acquired using back- scattered electrons in order to identify deteriorated areas. Maps were acquired using the intensity of the K α rays for the relevant chemical elements (Si, Ca, Mg, K), modifications being expected after the attack for these specific ones.

224 *2.3.3 X-ray diffraction (XRD) analyses*

225 In order to detect and identify the crystalline phases
 226 present and their possible in-core degree of penetra-
 227 tion, three holes were drilled at three successive dis-
 228 tances, from the sample’s edge to its center, using
 229 3 mm diameter drills, as shown in Fig. 8 of Appen-
 230 dix 1. Subsequently, the resulting cement powder
 231 was gathered for qualitative analysis by X-ray dif-
 232 fraction (XRD). The XRD measurements were per-
 233 formed using a PANalytical Empyrean diffractom-
 234 eter equipped with Co K α radiation and a PIXcel^{3D}
 235 detector. Current and voltage on the X-ray tube were
 236 30 mA and 40 kV, respectively. The diffractograms
 237 were acquired in the range of 2 θ from 4° to 76° with
 238 a step size of 0.013° 2 θ /s. Mineral identification was
 239 carried out using the HighScore Plus software with
 240 the crystallography open database (COD) [20–27].

241 *2.3.4 Thermogravimetric analysis (TGA–DTA)
 242 coupled with a mass spectrometer*

243 Using the resulting cement powder gathered from
 244 the drilling process described in the subSect. 2.3.3.,
 245 the thermogravimetric (TGA) and differential ther-
 246 mal (DTA) analysis for the identification of the dif-
 247 ferent phases, progressing from the edge of the sam-
 248 ple towards its center, was carried out in a dry argon
 249 atmosphere using a NETZSCH STA 409E simulta-
 250 neous thermal analyzer, performing both TGA and
 251 DTA simultaneously. The selected temperature ramp
 252 was 30–1250 °C, with an argon flow rate of 40 ml/
 253 min and a heating rate of 10 °C/min. All through the
 254 heating process, weight changes are generated by the
 255 loss of H₂O and CO₂ as the temperature increases.
 256 Emitted gas, H₂O, and CO₂ were monitored over time
 257 using a mass spectrometer, with 18.09 g/mol, and
 258 44.09 g/mol respectively used as molar masses.



259 2.3.5 μ -Raman spectroscopy

260 As shortly mentioned in the introduction, Raman
261 spectroscopy is now implemented in the characteriza-
262 tion of civil engineering materials, and in the continu-
263 ous monitoring of some of their evolution. In addition
264 to all the advantages that Raman spectroscopy offers,
265 such as being a non-destructive and rapid technique,
266 it has been found to successfully detect the sulfate
267 attack product in cementitious materials [28, 29].

268 Precise punctual measurements were conducted
269 along a radial line over a section of the samples (cf.
270 Figure 9 of Appendix 1) to enhance the investigation
271 of the mineralogical characterizations of the mortar
272 samples. The analyses were performed using two dif-
273 ferent instruments.

274 The first one was a BWTek iRaman spectrom-
275 eter operating with a 532 nm laser wavelength
276 and delivering nearly 50 mW power output. The
277 2048-pixel CCD detector provided spectra over the
278 150–4000 cm^{-1} spectral range with a resolution of
279 4 cm^{-1} . It was paired to a BAC151C microscope, and
280 spectral measurements were made through an $\times 50$
281 objective lens from Olympus. Both BWTek instru-
282 ments are managed by BWSpec 4.11_1 software.

283 The second spectrometer was a LabRAM HR800
284 spectrometer operating with a 514 nm laser wave-
285 length and delivering nearly 1 mW power output.
286 The instrument is optically coupled to a BX-model
287 microscope from Olympus, with a $\times 50$ (NA 0.75)
288 MPlanN objective. The diffraction-limited spot size is
289 then about 1 μm . The detector provided spectra over
290 the 50–4000 cm^{-1} spectral range with a resolution of
291 1 cm^{-1} . An XY-motorized stage allowed to taking of
292 in-line profiles and 2D mappings with a displacement
293 step as low as 1 μm . All devices are controlled by
294 LabSpec 6 software.

295 3 Results

296 3.1 In situ visual evolution monitoring

297 Photographs taken at each time scale provided an
298 overview of a qualitative visual evolution of the
299 cementitious materials, as shown in Fig. 3. Since
300 the very first sampling period (21 months), the dete-
301 rioration of all the specimens has been observed and
302 has evolved over the years. Indeed, according to the

literature with samples exposed to average H_2S con- 303
centrations of 5 and 100 ppm respectively [30, 31], 304
samples were expected to show much more notice- 305
able visual deterioration after 44 months of exposure. 306
Therefore, it can be noticed that the mortars are mod- 307
erately well preserved and that this limitation of deg- 308
radation can be strongly linked to their exposure to a 309
very low concentration of H_2S . 310

311 Based on the visual characteristics only, through-
312 out the study period, the changes in all samples were
313 characterized by the presence of white crystals and
314 brownish deposits. At the end of the 44 months, the
315 specimens had somewhat darkened and showed some
316 deterioration marks, notably the growth of expansive
317 products.

318 Alongside a visual inspection of the degradation,
319 sample weights were measured during the *in-situ*
320 exposure period. All the examined mortars exhibited
321 identical behavior, as illustrated in Fig. 4. Over the
322 first 21 months, a weight gain is recorded, which can
323 be linked to the accumulation of water in the pores
324 of the mortar specimens and the formation of sulfide
325 reaction products, followed by a slight weight loss.
326 It is crucial to highlight that all the types of cement
327 used in the study showed a similar variation in weight
328 percentage.

329 The examination of pH values throughout the
330 study period revealed a significant drop in the sur-
331 face pH, from its initial alkaline value to an acidic
332 value after 21 months, followed by stabilization in the
333 4–6 range over the subsequent months. This pattern
334 reflects the results documented in existing literature
335 [30–32].

336 Furthermore, the investigation of the diameter
337 evolution over the 44 months did not reveal any

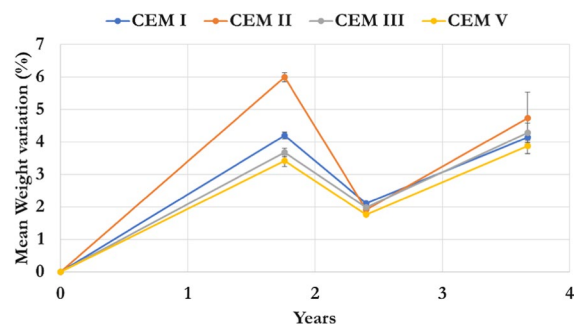


Fig. 4 Mean weight variation of mortar samples exposed for 44 months at a low H_2S concentration



338 significant change for all the specimens. The percent
339 change in diameter ranged from 0 to 0.7% of expansion
340 over the study period, which is consisted with
341 the visual observations that did not reveal any notice-
342 able expansion of the mortars.

343 3.2 Chemical profile maps determination

344 SEM observations and elemental map investiga-
345 tions facilitated the identification of diverse elemen-
346 tal chemical distributions and sample zonation. Fig-
347 ures 10–13 in the Appendix illustrate the multimodal
348 analysis of the mortar specimens, presenting visualiza-
349 tions of cross-sections obtained using KEYENCE,
350 SEM imaging of half the section and the selected sec-
351 tion to be analyzed with EDS. The interpretation of
352 chemical variations relied on the distribution of ele-
353 ments compounds determined through EDS analysis.
354 The identification of various microstructural zones
355 in all examined deteriorated mortar samples closely
356 aligns with previous findings [32–35]. Furthermore, a
357 consistent behavior was observed across all samples,
358 attributed to their shared composition of Portland
359 cement. This emphasizes the reliability of the results
360 and underscores a uniform response to selected envi-
361 ronmental factors.

362 Four distinct zones have been distinguished in
363 these samples through meticulous analysis, as illus-
364 trated in Figs. 5 and 6. Each zone reveals unique fea-
365 tures indicating specific compositional, mineralogical,
366 and microstructural characteristics.

367 The first zone, prominently visible in the SEM
368 images, consisted of a strongly altered area. This
369 near-surface zone is locally enriched in sulfur and
370 calcium (cf. zone 1 in Fig. 5), precipitating mainly
371 along long reticulated crack systems.

372 Moving on to a second zone, its composition dif-
373 fered notably from the first, with a porous structure
374 characterized by the presence of Si and the depletion
375 of the S and Ca elements, creating a distinctive void
376 in the elemental composition. Additionally, this zone
377 is characterized by the absence of anhydrous phases
378 (such as C₂S, C₃S, etc.). In the backscatter images,
379 anhydrous phases typically appear as white elements;
380 however, they are absent in this specific zone of the
381 section. This particular zone can be most precisely
382 described as an outer transition zone, representing a
383 boundary between the strongly deteriorated external
384 zone and the slightly deteriorated internal zone.

The third zone can be most accurately described 385
as an inner transition zone, marked by the accumu- 386
lation of K and Mg elements, followed by the suc- 387
cessive incorporation of S and Ca. Furthermore, 388
this zone can be subdivided into two distinct inter- 389
zones, labeled 3a and 3b. These sub-zones are 390
clearly differentiated by the absence of anhydrous 391
phases in zone 3a and their presence in zone 3b, 392
with an additional layer of complexity to the min- 393
eralogical composition in this transitional region. 394
This zone further contributes to the comprehensive 395
understanding of the sample's heterogeneity. 396

397 These deteriorated layers probably consist of
398 newly formed calcium sulfates. These layers are
399 identified by regions where calcium and sulfur have
400 accumulated. Additionally, they are less defined
401 layers containing silicon. However, in cases where
402 only sulfur was detected in the elemental distribu-
403 tion images, the presence of elemental sulfur was
404 probable.

405 Lastly, a fourth zone, which can be described as
406 the pristine zone, indicates that its mineralogical
407 composition has remained relatively unchanged.
408 This zone features an abundance of anhydrous
409 phases (such as C₂S, C₃S, slag, ...) identifiable
410 on BSE images. The presence of anhydrous phases
411 indicates a chemical reaction of the water with the
412 initial cement, potentially contributing to the zone's
413 resistance to the deleterious effects of H₂S. Indeed,
414 the distinction between all the zones can be effec-
415 tively discerned through the variations in texture
416 from one zone to its neighbors.

417 From the results illustrated in Fig. 5, the CEM I
418 sample features all four of the identified zones. On
419 the other hand, the CEM III and CEM V samples
420 exhibit similar zonation, whereby the second zone
421 is notably lacking. Conversely, the CEM II sample
422 presents a marked change in element distribution,
423 as illustrated in Fig. 6. Particularly in its third zone,
424 where the element sulfur is notably absent.

425 With these findings and ImageJ software [36],
426 measurements of minimum and maximum values
427 were taken for each zone of the samples for com-
428 parative analysis, as shown in Table 1. The results
429 reveal that all the samples present deteriorated lay-
430 ers in varying degrees of proximity. Remarkably, **AQ4**
431 the CEM II sample was found to be the most deter-
432 iorated of all the Portland cement samples studied
433 (Table 2).



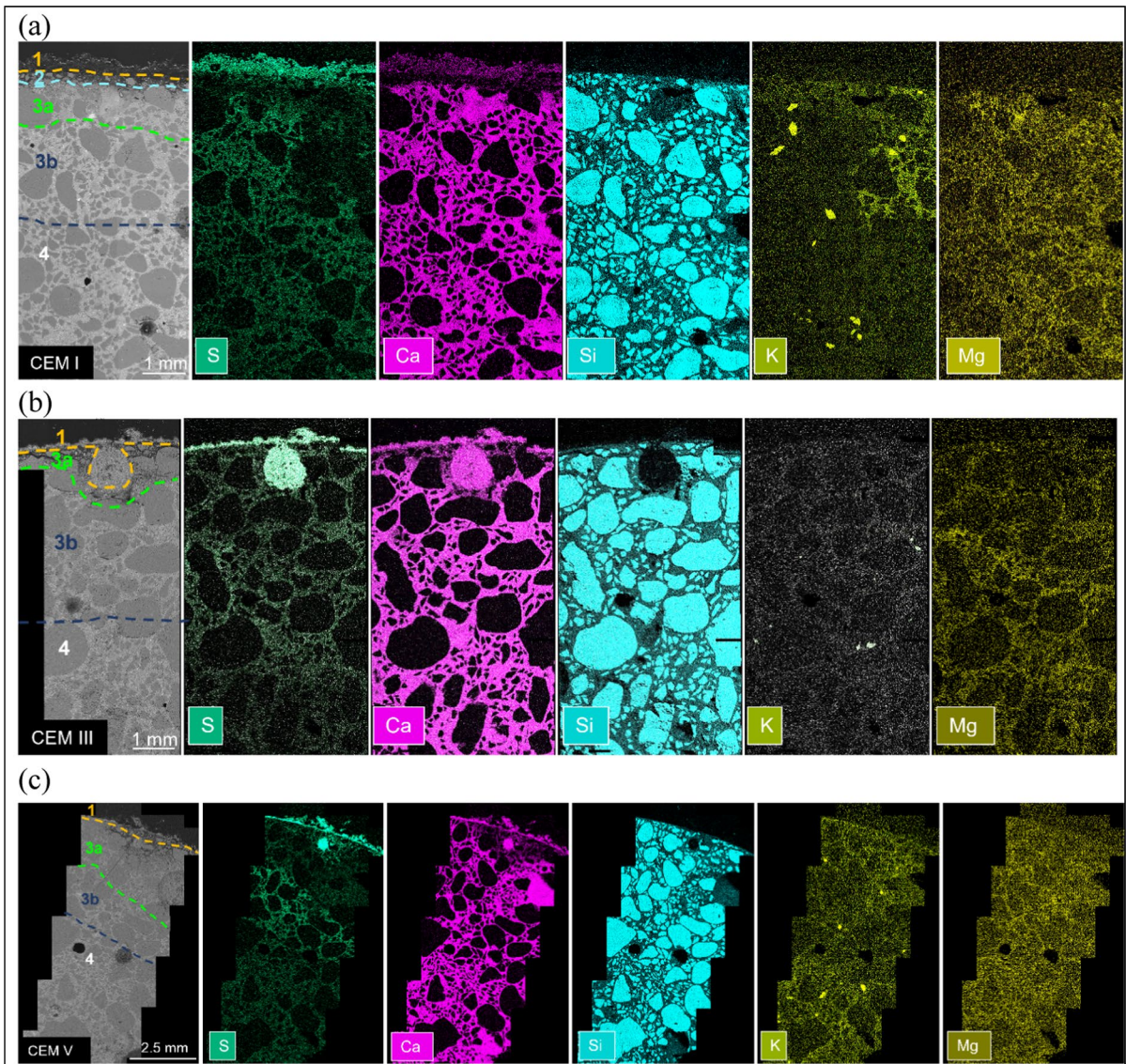


Fig. 5 High resolution and elemental distribution images of S, Ca, Si, K, and Mg of cross-sections in **a** CEM I, **b** CEM III, and **c** CEM V samples, revealing the varied zones from the exterior deteriorated zone to the interior pristine zone

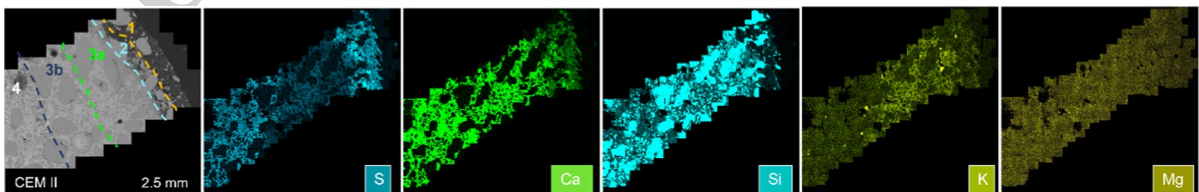


Fig. 6 High resolution and elemental distribution images of S, Ca, Si, K, and Mg of cross-sections in the CEM II sample, revealing the varied zones from the exterior deteriorated zone to the interior pristine zone



Table 2 Alteration zone thickness variations for various cement types in mm (min–max)

	Zone 1	Zone 2	Zone 3a	Zone 3b
CEM I	0.2–0.5	0.2–0.3	0.9–1.1	1.9–2.3
CEM II	0.8–1.4	0.6–0.7	1.7–2.1	1.7–2.4
CEM III	0.3–0.9	NA	0.2–0.3	2.623.2
CEM V	0.2–0.7	NA	1.9–2.1	1.9–2.1

3.3 Mineralogical characterization

XRD (X-ray Diffraction) and TGA (Thermogravimetric Analysis), analyses were carried out for the mineralogical characterization of the cementitious samples into the depth of the materials constituting the samples. Nevertheless, considering the information presented in Sect. 3.2 and the fact that the holes in the samples were obtained using 3 mm drills, it can be asserted that the first hole falls within the three pre-defined zones. Consequently, differentiation of results based on specific zones, according to XRD and TGA, is not feasible. However, it can be considered that the first hole occurred in the deteriorated part of the sample (zones 1, 2, 3a, and 3b previously described in Sect. 3.2 and shown in Figs. 5 and 6), while the other two occurred in the intact zone (zone 4 previously described in Sect. 3.2.).

Qualitative XRD analyses of the resulting cement powder showed the quartz (peak at 3.34 Å) contained in the sand to be the main crystallized phase for all the holes of the four cement types.

For the Ordinary Portland cement sample CEM I, XRD results revealed the presence of the semi-hydrated phase of gypsum ‘bassanite’ ($\text{CaSO}_4 \cdot 0.5\text{H}_2\text{O}$, peak at 3.00 Å) and calcite (CaCO_3 , peak at 3.04 Å), in the altered layer of the sample indicating the local variation in the mineralogical composition of the sample due to the biogenic H_2S attack. Furthermore, portlandite (peak at 2.63 Å) was detected throughout the core of the sample. Figure 14 of Appendix 1 shows the diagrams of the three holes of the CEM I specimen.

For the CEM II and CEM III samples, XRD analyses confirmed the predominance of quartz, but other phases such as calcite and portlandite were also identified throughout the radial line of the samples. Moreover, vaterite (peak at 3.29 Å) was also detected in the CEM III sample.

Nevertheless, for the CEM V sample, no other phases apart from quartz were detected in the intact zone of the sample. However, in the deteriorated zone, gypsum (peaks at 7.62 and 4.27 Å) and calcite were identified.

On the other side, the TGA-MS results for all the samples revealed the presence of four distinctive stages of weight loss over the entire temperature range, spanning from 30 to 1250 °C.

The initial weight loss, occurring between room temperature and 220 °C, was attributed to the evaporation of all free water and of water from the C–S–H and ettringite components. The following weight loss, between 380 and 500 °C, is mainly due to the liberation of water during the dehydration process of portlandite. This percentage weight loss can be effectively used to estimate the portlandite content of samples. With the third stage of weight loss, which takes place between 700 and 800 °C, CO_2 is released, making it possible to estimate the CaCO_3 content in the mortar samples. The final weight loss observed above 1000 °C is attributed to the release of SO_3 , which originates from the sulfates contained in the gypsum and ettringite due to the H_2S attack in the mortar samples [9].

Taking all the findings together, it is confirmed that the samples have undergone an alteration with a mineralogical modification. However, it should be noted that this change was not as severe as that previously recorded for samples heavily exposed to H_2S [8–10, 37]. The mineral phases identified in the samples of this study suggest alteration, but to a lesser degree, underlining the importance of environmental conditions in the mineral alteration process.

Moreover, these results demonstrate that after 44 months of in-situ exposure in a sewer environment, all Portland cement-based mortars contain portlandite all over the different zones of the samples. This finding can be justified by the low concentration of H_2S in the exposition zone, as the reduced presence of hydrogen sulfide leads to a less aggressive chemical environment.

3.4 Mineralogical characterization by micro-Raman spectroscopy

Among the different methods assessed, the Raman spectroscopy analysis consistently identified the presence of gypsum in the deteriorated layers of all



519 the specimens under investigation. Notably, gyp-
520 sum formation is characteristic of the sulfate attack
521 of a cementitious material. This material has a spe-
522 cific peak at 1003 cm^{-1} , as indicated in the literature
523 [38]. A photograph of an altered zone of a polished
524 section of the exposed CEM V sample is shown in
525 Fig. 7a. Additionally, Fig. 7b presents its spectral
526 analysis over two spectral ranges (laser at 514 nm,
527 25-s acquisition time, and averaged over 4 spectra),
528 with an emphasis on the intensification characteristic
529 of the gypsum spectrum. It is crucial to outline that
530 the observed vibrational modes closely align with the
531 literature data [29, 37, 39, 40].

532 Starting with the CEM I specimen exposed to the
533 H_2S -enriched environment, alongside gypsum, the
534 analysis revealed the presence of ettringite and two
535 calcium carbonate polymorphs (calcite and vaterite,
536 with a main intense peak respectively at 1085 cm^{-1}
537 and $1077\text{--}1090\text{ cm}^{-1}$) [29, 41–43]. Ettringite and
538 gypsum were detected in the altered zone, and
539 according to the literature, they have been identified
540 as the main reason for the sulfate attack damage [29,
541 44]. However, calcium carbonate was detected along
542 the radial line of the sample.

543 Moving on to the CEM II specimen, calcite was
544 identified in all the measurements taken, indicating its
545 consistent presence. The existence of this supplemen-
546 tary phase within the alteration layer suggests that the
547 formation of gypsum might have arisen either from
548 calcium ions present in the constituent phases of the
549 cementitious matrix (portlandite and C–S–H) or from
550 calcite. Moreover, it is worth noting that calcite is
551 consistently observed in all the samples and at greater
552 depths within the mortars. The presence of CaCO_3 in

the samples' sections could also be attributed to an
unavailable carbonation occurring once the inner part
of the samples had been exposed to the atmosphere
and during the polishing process, despite cautious
storage conditions.

For the CEM III sample, the sulfite mineral hanne-
bachite was also detected at the surface of the mortar
sample [45]. As per prior studies, Pons et al. [37] also
identified hannebachite in a previous CEM III mortar
sample.

Lastly, in the case of the CEM V specimen, ettrin-
gite and calcite were also detected in addition to
gypsum.

All these findings reinforce the spectroscopic tech-
nique's importance for assessing the cementitious
matrix's bio-alteration, but also about its spatial reso-
lution with respect to TGA and XRD.

4 Discussion

This study highlights the significant synergies arising
from the utilization of diverse analytical techniques.
While each method provided valuable data inde-
pendently, the true strength of the results emerged
when considering the correlations and relationships
revealed through their collective examination. The
interconnections observed among XRD, SEM–EDS,
TGA–MS, μ -Raman spectroscopy, and in situ moni-
toring collectively present a comprehensive portrayal
of the impact of low H_2S concentrations on cementi-
tious materials in sewage systems. These techniques,
when integrated, offer a holistic view, uncovering
mineralogical modifications and chemical alterations

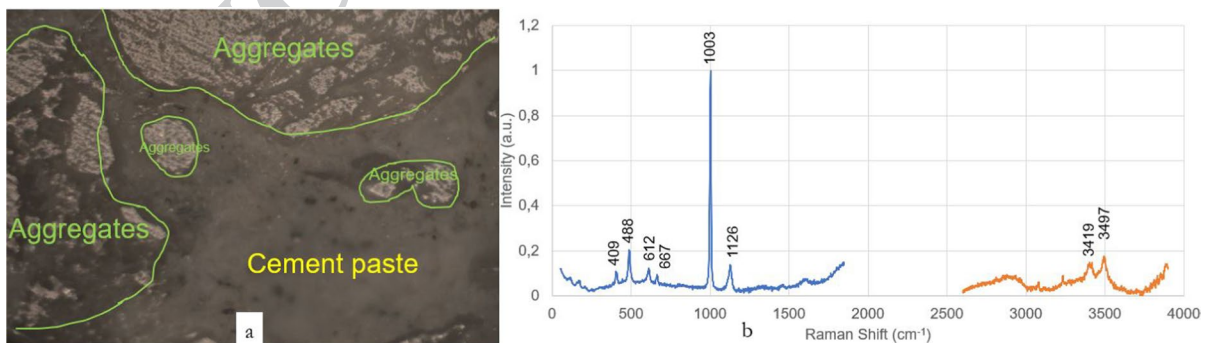


Fig. 7 a Photograph in reflected light of a CEM V altered zone, and b a normalized Raman spectrum (obtained with the LabRAM HR800 spectrometer) after 44 months of exposure in a sewage system



584 within the cementitious matrix. This multifaceted
585 approach proves crucial, as it goes beyond the limita-
586 tions of any single analytical method.

587 The intricate nuances of material degradation in
588 cement samples exposed to an H₂S-enriched atmos-
589 phere in wastewater networks are brought to light
590 through meticulous scanning electron microscopy
591 observations. The SEM reveals a fascinating diversity
592 within the deteriorated portions of the sample, where
593 different zones, each characterized by distinct chemi-
594 cal features and sizes, emerge even in the thinnest
595 sections. This microscale analysis, with its capacity
596 to discern minute variations, surpasses the capabili-
597 ties of traditional tools such as TGA and XRD. The
598 revelation of specific characteristics within each zone,
599 despite their thinness, underscores the non-uniform
600 nature of the degradation process. It becomes evi-
601 dent that a comprehensive understanding of this com-
602 plex interaction necessitates a diversified analytical
603 approach. This exploration not only highlights the
604 limitations of singular analytical tools but emphasizes
605 the imperative role of complementary techniques.

606 In this context, SEM, with its precision at the
607 microscale, and Raman spectroscopy stand out as piv-
608 otal contributors. Their integration facilitates a more
609 holistic analysis, providing unparalleled insights into
610 the intricate interplay between cement samples and
611 H₂S. This synergy between SEM and Raman spec-
612 troscopy transcends the individual constraints of each
613 technique, offering a comprehensive understanding
614 of the material deterioration process. In essence, this
615 approach broadens the horizons of material science,
616 demonstrating the indispensability of diverse analyti-
617 cal tools in unraveling the complexities of biodegra-
618 dation in cement exposed to environmental stressors.

619 In this research, the analysis of element distri-
620 bution in deteriorated concrete layers revealed a
621 dynamic system influenced by pH and diffusion of
622 elements into the cement matrix. It revealed a clear
623 sequence of element accumulation closely linked to
624 pH levels, the dissolution and precipitation of solids,
625 some variations in chemical compositions of cementi-
626 tious binders, and the spatial distribution of bacteria
627 present in the wastewater.

628 The strongly deteriorated surface layer (zone
629 1) extending from 0.2 to 1.4 cm featured a com-
630 position comprising filamentous structures
631 composed of S and Ca. These structures repre-
632 sented the precipitation of secondary sulfate

salts, including gypsum (CaSO₄·2H₂O), ettrin- 633
gite (Ca₆Al₂(SO₄)₃(OH)₁₂·26H₂O), anhydrite 634
(CaSO₄), hannebachite (CaSO₃·H₂O), and bassanite 635
(CaSO₄·0.5H₂O). The formation of hannebachite and 636
bassanite can be explained by cycles of humidifica- 637
tion and drying, leading to fluctuating SO₄²⁻ and H₂O 638
activities in the mortar's interstitial solutions. Si-rich 639
layers, on the other hand, consisted of amorphous 640
silica. 641

The transition zone, segmented into three distinct 642
inter zones (Zones 2, 3a, and 3b) between strongly 643
deteriorated and intact concrete, was bounded within 644
a range of 3–5 mm. This led to dynamic dissolution 645
and precipitation of individual phases, as shown by 646
the concentrations of individual elements in Figs. 5 647
and 6. The interface between Zones 2 and 3 in the 648
transition zone was characterized by a reduction in Ca 649
concentration following acid penetration. Meanwhile, 650
a simultaneous process of sulfate incorporation along 651
the grain boundaries was observed, suggesting that 652
this could be associated with the interfacial transition 653
zone and its higher portlandite content (Ca(OH)₂) 654
[46]. This resulted in the microstructural deteriora- 655
tion of the cement matrix through the formation of 656
expansive sulfate phases [47]. From the very initial 657
edge of zone 3, Mg accumulation occurred as a result 658
of the precipitation of Mg hydroxides, such as brucite 659
(Mg(OH)₂). In this process, hydroxide (OH⁻) diffused 660
from alkaline areas in the intact mortar, while diffu- 661
sion of Mg ions was induced by Mg precipitation and 662
the associated concentration gradient. Given that the 663
stability of Mg-containing precipitates is limited to 664
strongly alkaline conditions, the cessation of Mg pre- 665
cipitation marks the end of zone 3. Mg thickness and 666
concentrations in the accumulation zone have been 667
found to correlate directly with the dominant pH gra- 668
dient, making them indicative of the rate of deteriora- 669
tion [33, 48]. Furthermore, in this transition zone, a 670
noticeable accumulation of potassium (K) occurs in 671
the elemental distribution (Figs. 5 and 6). Analysis 672
of the compositional data suggests that these addi- 673
tional precipitates could be identified as (K-alum) 674
(KAl(SO₄)₂·12H₂O), syngenite (K₂Ca(SO₄)₂·H₂O), 675
or alunite (KAl₃(SO₄)₂(OH)₆ that is also affected by 676
the alkaline leaching rate [33, 49]. 677

The intact pristine zone (zone 4), identified as 678
the inferior zone, features a matrix mainly made 679
up of calcium- and silicon-rich phases, including 680
portlandite and hydrated calcium silicates (C–S–H 681



682 phases) as well as anhydrous grains. This matrix
683 envelops silica and carbonate aggregates. In addition,
684 various calcium carbonate polymorphs, such as
685 calcite and vaterite, have been detected in this zone.

686 5 Conclusion

687 This research has illuminated the significant impact of
688 low H_2S concentrations on cementitious materials in
689 sewage systems. This impact, although often overlooked,
690 plays a fundamental role in the degradation process of
691 the cementitious materials that constitute these systems.
692 Previous research has focused primarily on high H_2S
693 concentrations, yet this study unveiled the subtle but
694 consequential effects of low H_2S levels. By combining
695 a full range of analytical techniques, including XRD,
696 SEM-EDS, TGA-DTA, and Raman spectroscopy, in
697 conjunction with continuous weight measurements and
698 visual observations, several significant breakthroughs
699 were achieved.

700 On the visual side, samples subjected to low H_2S
701 concentrations showed no dramatic indications of
702 deterioration compared to those exposed to more
703 harsh environmental conditions. However, the
704 real significance of these results lies beneath the
705 surface, since the cementitious materials underwent
706 considerable mineralogical alterations.

707 Most notably, these analyses highlighted the presence
708 of several minerals in the mortar samples, underscoring
709 the extent of the changes observed. In particular,
710 bassanite and hannebachite, which are precursors
711 to gypsum and have not been identified in materials
712 subjected to higher levels of H_2S , were discovered.
713 Moreover, gypsum, ettringite, elemental sulfur,
714 and various polymorphs of calcium carbonate were
715 identified along a radial line from the edge to the core
716 of the samples. These mineralogical transformations
717 emphasize the complex interplay between low H_2S
718 concentrations and the composition of cementitious
719 materials, which, although less visible on the surface,
720 have a considerable impact on their long-term durability.

721 Furthermore, magnesium and potassium were
722 detected in the altered layers following the chemical
723 reactions of the Portland cement-based mortars at
724 low H_2S levels. The unexpected existence of these
725 components underlines both the complexity and the
726 subtlety of biogenic sulfuric attacks on cementitious
727 materials.

Remarkably, this study showed no real difference 728
in the durability of the various cement-based paste 729
samples used. The absence of any significant dif- 730
ferentiation in resistance to low H_2S concentrations 731
suggests that there is no distinct hierarchy in the clas- 732
sification of pastes according to their degree of resist- 733
ance. It is noteworthy, however, that the CEM II sam- 734
ple revealed a slightly thicker deteriorated layer than 735
the others, pointing to a nuanced aspect in the perfor- 736
mance of these cement pastes. 737

To conclude, the outcomes of this study are very 738
consistent with the existing literature on studies at 739
high concentrations of H_2S , highlighting the crucial 740
importance of considering low H_2S levels when 741
assessing the durability of cementitious matrices in 742
wastewater systems. Moreover, this study highlights the 743
importance of using very precise analytical techniques, 744
such as micro-Raman and SEM-EDS, to thoroughly 745
assess all the layers arising during the biodeterioration 746
process. 747

Acknowledgements "This project has received funding from 748
the European Union's Horizon 2020 research and innovation pro- 749
gramme under the Marie Skłodowska-Curie COFUND grant 750
agreement No 101034248." The authors gratefully acknowledge 751
Gwénaél GOUADEC for his invaluable assistance in conducting 752
several critical Raman measurements, Béatrice Desrues for her 753
invaluable assistance in conducting the SEM-EDS acquisition, and 754
Céline Briand for her technical assistance at SIAAP. 755

Funding HORIZON EUROPE Marie Skłodowska-Curie 756
Actions, 101034248, Janette Ayoub 757

Data availability Data will be provided on request. 758

Appendix 1 759

See Figs. 8, 9, 10, 11, 12, 13 and 14 760

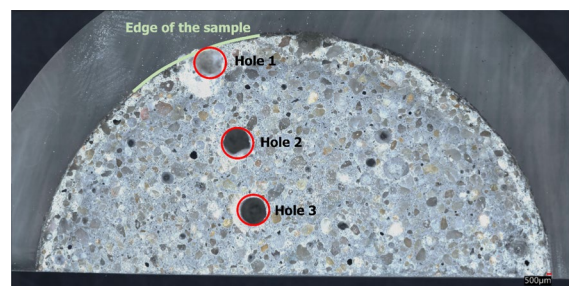


Fig. 8 A Keyence figure of a CEM V sample showing holes drilled at successive distances from the edge



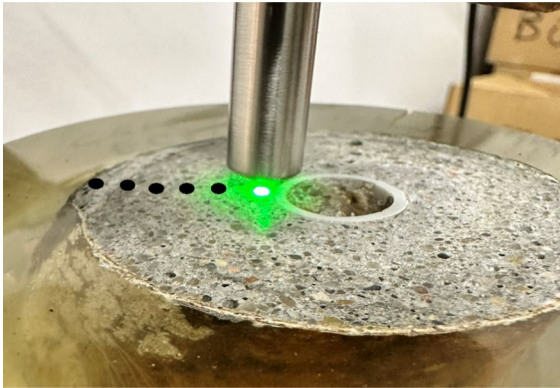
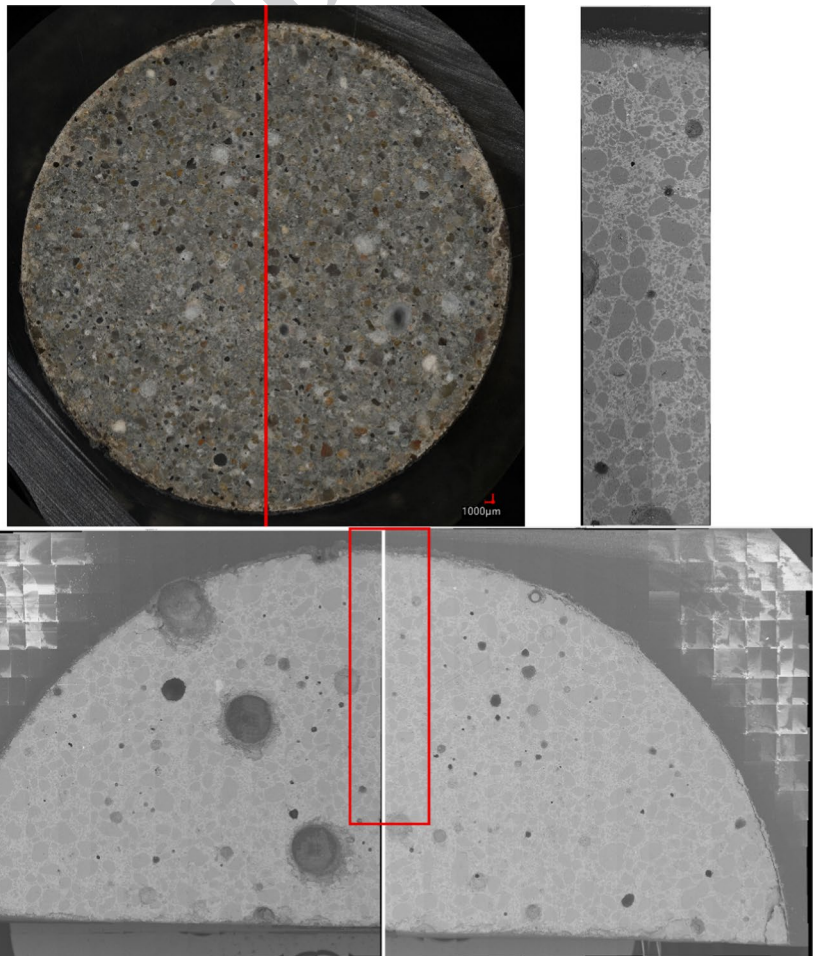


Fig. 9 Example of punctual measurements sequencing in μ -Raman spectroscopy. The green dot signifies the initial laser acquisition point, while the multiple black dots illustrate the subsequent acquisitions

Fig. 10 Analysis of CEM I Mortar: **a** Cross section visualization with Keyence, **b** Back scatter image, and **c** EDS elemental analysis selection



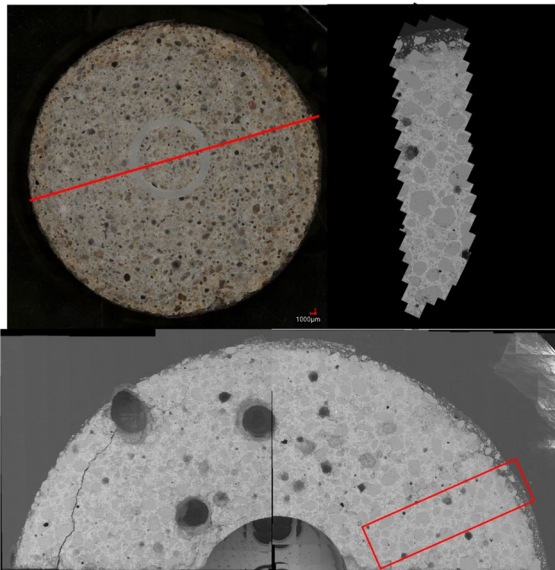


Fig. 11 Analysis of CEM II mortar: cross section visualization with Keyence, SEM imaging, and EDS elemental analysis selection

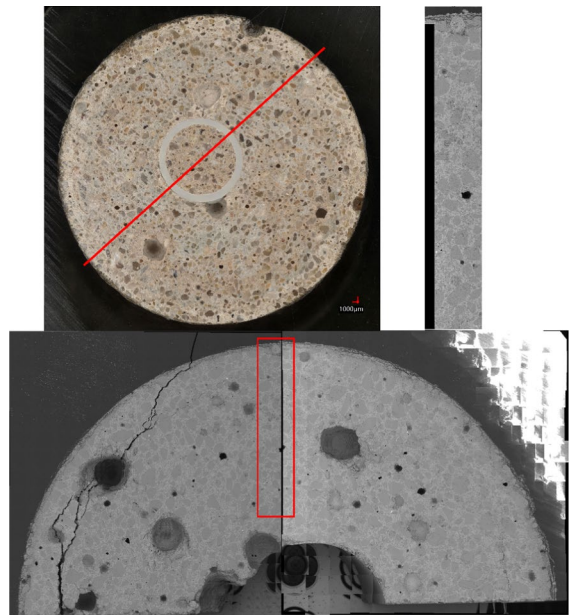
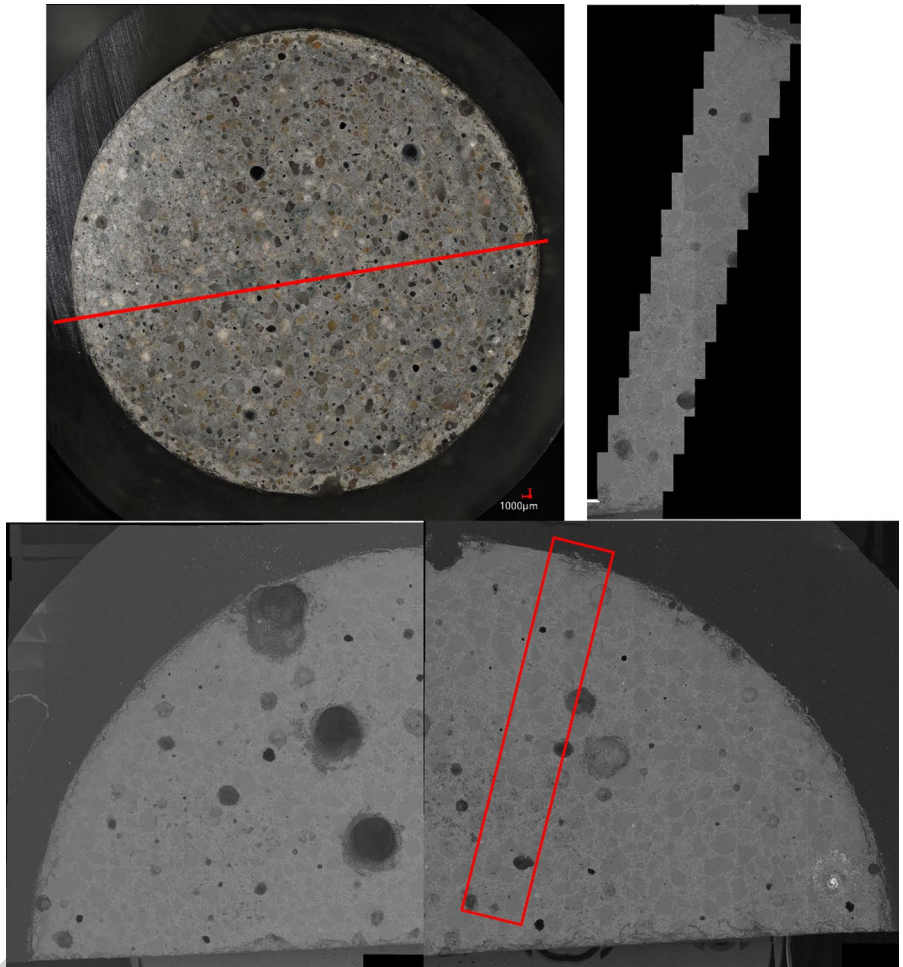


Fig. 12 Analysis of CEM III mortar: Cross section visualization with Keyence, SEM imaging, and EDS elemental analysis selection

UNCORRECTED



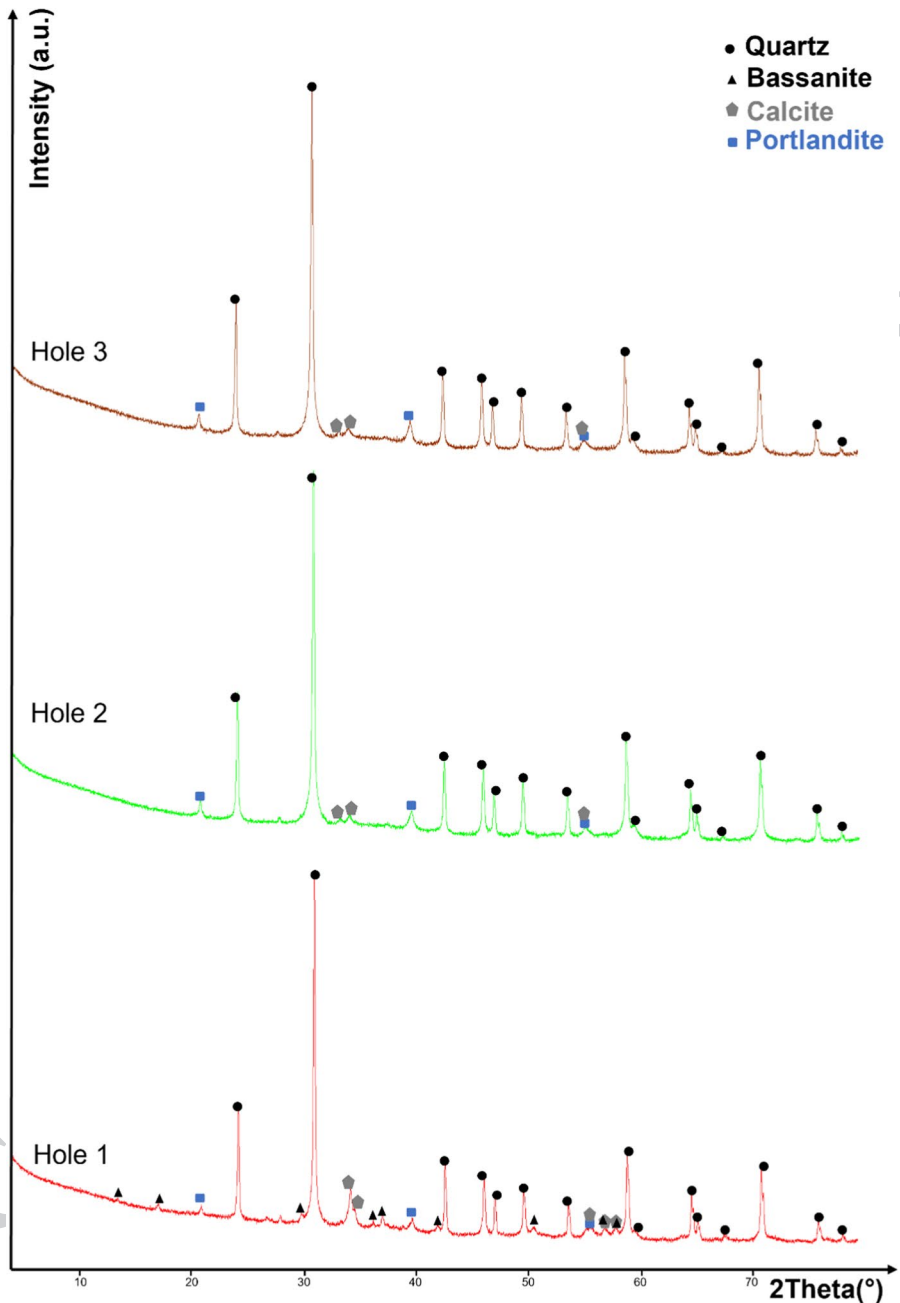
Fig. 13 Analysis of CEM V mortar: Cross section visualization with Keyence, SEM imaging, and EDS elemental analysis selection



UNCORRECTED



Fig. 14 RDX diagram of the three holes in the CEM I specimen



761 References

- 762 1. Kaempfer W, Berndt M (1999) Estimation of service life
763 of concrete pipes in sewer networks. *Durab Build Mater*
764 *Compon* 8:36–45
- 765 2. Monteny J, Vincke E, Beeldens A et al (2000) Chemical,
766 microbiological, and in situ test methods for biogenic sulfuric
767 acid corrosion of concrete. *Cem Concr Res* 30:623–
768 634. [https://doi.org/10.1016/S0008-8846\(00\)00219-2](https://doi.org/10.1016/S0008-8846(00)00219-2)
- 769 3. O'Connell M, McNally C, Richardson MG (2010) Bio-
770 chemical attack on concrete in wastewater applications:
771 a state of the art review. *Cement Concr Compos* 32:479–
772 485. <https://doi.org/10.1016/j.cemconcomp.2010.05.001>
- 773 4. Stokbro Jensen H (2009) Hydrogen sulfide induced
774 concrete corrosion of sewer networks: Ph. D. disserta-
775 tion. Section of environmental engineering, Aalborg
776 University
- 777 5. Okabe S, Odagiri M, Ito T, Satoh H (2007) Succession
778 of sulfur-oxidizing bacteria in the microbial community



- on corroding concrete in sewer systems. *Appl Environ Microbiol* 73:971–980. <https://doi.org/10.1128/AEM.02054-06>
6. Melchers RE, Bond P (2009) Factors involved in the long term corrosion of concrete sewers
7. MaGD G-P, Bielefeldt A, Ovtchinnikov S et al (2010) Biogenic sulfuric acid attack on different types of commercially produced concrete sewer pipes. *Cem Concr Res* 40:293–301. <https://doi.org/10.1016/j.cemconres.2009.10.002>
8. Herisson J (2012) Biodétérioration des matériaux cimentaires dans les ouvrages d'assainissement: étude comparative du ciment d'aluminate de calcium et du ciment Portland
9. Grandclerc A (2017) Compréhension des mécanismes de biodétérioration des matériaux cimentaires dans les réseaux d'assainissement: étude expérimentale et modélisation
10. Grengg C, Mittermayr F, Ukrainczyk N et al (2018) Advances in concrete materials for sewer systems affected by microbial induced concrete corrosion: a review. *Water Res* 134:341–352. <https://doi.org/10.1016/j.watres.2018.01.043>
11. Aboulela A (2022) Study of the resistance to biodeterioration of innovative low-carbon cementitious materials for application in sewer networks
12. Herisson J, van Hullebusch ED, Moletta-Denat M et al (2013) Toward an accelerated biodeterioration test to understand the behavior of Portland and calcium aluminate cementitious materials in sewer networks. *Int Biodeterior Biodegradation* 84:236–243. <https://doi.org/10.1016/j.ibiod.2012.03.007>
13. Wu M, Wang T, Wu K, Kan L (2020) Microbiologically induced corrosion of concrete in sewer structures: a review of the mechanisms and phenomena. *Constr Build Mater* 239:117813. <https://doi.org/10.1016/j.conbuildmat.2019.117813>
14. Haque F, Santos RM, Chiang YW (2019) Using non-destructive techniques in mineral carbonation for understanding reaction fundamentals. *Powder Technol* 357:134–148. <https://doi.org/10.1016/j.powtec.2019.08.089>
15. Potgieter-Vermaak SS, Potgieter JH, Van Grieken R (2006) The application of Raman spectrometry to investigate and characterize cement, Part I: a review. *Cem Concr Res* 36:656–662. <https://doi.org/10.1016/j.cemconres.2005.09.008>
16. Black L (2009) Raman spectroscopy of cementitious materials. In: Yarwood J, Douthwaite R, Duckett S (eds) *Spectroscopic properties of inorganic and organometallic compounds*. Royal Society of Chemistry, Cambridge, pp 72–127
17. Prieto-Taboada N, Larrañaga A, Gómez-Laserna O et al (2015) The relevance of the combination of XRD and Raman spectroscopy for the characterization of the CaSO₄-H₂O system compounds. *Microchem J* 122:102–109. <https://doi.org/10.1016/j.microc.2015.04.010>
18. Marchetti M, Mechling J-M, Janvier-Badosa S, Offroy M (2023) Benefits of chemometric and Raman spectroscopy applied to the kinetics of setting and early age hydration of cement paste. *Appl Spectrosc* 77:37–52. <https://doi.org/10.1177/00037028221135065>
19. FD (2022) P18–011. In: *Afnor editions*. <https://www.boutique.afnor.org/fr-fr/norme/fd-p18011/beton-definition-et-classification-des-environnements-chimiquement-agressif/fa204582/328696>. Accessed 4 Dec 2023
20. Downs RT, Hall-Wallace M (2003) The American mineralogist crystal structure database. *Am Mineral* 88:247–250
21. Gražulis S, Chateigner D, Downs RT et al (2009) Crystallography open database – an open-access collection of crystal structures. *J Appl Cryst* 42:726–729. <https://doi.org/10.1107/S0021889809016690>
22. Gražulis S, Daškevič A, Merkys A et al (2012) Crystallography open database (COD): an open-access collection of crystal structures and platform for worldwide collaboration. *Nucleic Acids Res* 40:D420–D427. <https://doi.org/10.1093/nar/gkr900>
23. Gražulis S, Merkys A, Vaitkus A, Okulič-Kazarinas M (2015) Computing stoichiometric molecular composition from crystal structures. *J Appl Cryst* 48:85–91. <https://doi.org/10.1107/S1600576714025904>
24. Merkys A, Vaitkus A, Butkus J et al (2016) COD::CIF::parser: an error-correcting CIF parser for the Perl language. *J Appl Cryst* 49:292–301. <https://doi.org/10.1107/S1600576715022396>
25. Quirós M, Gražulis S, Girdzijauskaitė S et al (2018) Using smiles strings for the description of chemical connectivity in the crystallography open database. *J Cheminform* 10:23. <https://doi.org/10.1186/s13321-018-0279-6>
26. Vaitkus A, Merkys A, Gražulis S (2021) Validation of the crystallography open database using the crystallographic information framework. *J Appl Cryst* 54:661–672. <https://doi.org/10.1107/S1600576720016532>
27. Merkys A, Vaitkus A, Grybauskas A et al (2023) Graph isomorphism-based algorithm for cross-checking chemical and crystallographic descriptions. *J Cheminform* 15:25. <https://doi.org/10.1186/s13321-023-00692-1>
28. Gutierrez RMP (2017) Chapter 2 - A novel approach to the oral delivery of bionanostructures for systemic disease
29. Tang C, Ling T-C, Mo KH (2021) Raman spectroscopy as a tool to understand the mechanism of concrete durability—a review. *Constr Build Mater* 268:121079. <https://doi.org/10.1016/j.conbuildmat.2020.121079>
30. Herisson J, Guéguen-Minerbe M, Van Hullebusch ED, Chaussadent T (2014) Behaviour of different cementitious material formulations in sewer networks. *Water Sci Technol* 69:1502–1508. <https://doi.org/10.2166/wst.2014.009>
31. Herisson J, Guéguen-Minerbe M, Van Hullebusch ED, Chaussadent T (2017) Influence of the binder on the behaviour of mortars exposed to H₂S in sewer networks: a long-term durability study. *Mater Struct* 50:8. <https://doi.org/10.1617/s11527-016-0919-0>
32. Pons T, Gueguen M, Grandclerc A et al (2018) Field investigation of cementitious materials durability in sewer environment
33. Grengg C, Mittermayr F, Koraimann G et al (2017) The decisive role of acidophilic bacteria in concrete sewer networks: a new model for fast progressing microbial



- 896 concrete corrosion. *Cem Concr Res* 101:93–101. <https://doi.org/10.1016/j.cemconres.2017.08.020>
- 897
- 898 34. Grengg C, Ukrainczyk N, Koraimann G et al (2020) Long-term in situ performance of geopolymer, calcium aluminate and Portland cement-based materials exposed to microbially induced acid corrosion. *Cem Concr Res* 131:106034. <https://doi.org/10.1016/j.cemconres.2020.106034>
- 900
- 901
- 902
- 903
- 904 35. Grengg C, Koraimann G, Ukrainczyk N et al (2021) Cu- and Zn-doped alkali activated mortar – properties and durability in (bio)chemically aggressive wastewater environments. *Cem Concr Res* 149:106541. <https://doi.org/10.1016/j.cemconres.2021.106541>
- 905
- 906
- 907
- 908
- 909 36. Schneider CA, Rasband WS, Eliceiri KW (2012) NIH Image to ImageJ: 25 years of image analysis. *Nat Methods* 9:671–675. <https://doi.org/10.1038/nmeth.2089>
- 910
- 911
- 912 37. Pons T, Fourdrin C, Grandclerc A et al (2018) Mineralogical characterization of the alteration layer of chemically and biologically altered cementitious materials
- 913
- 914
- 915 38. Chukanov NV, Vigasina MF (2020) *Vibrational (infrared and Raman) spectra of minerals and related compounds*. Springer International Publishing, Cham
- 916
- 917
- 918 39. Bensted J (1976) Uses of Raman spectroscopy in cement chemistry. *J Am Ceram Soc* 59:140–143. <https://doi.org/10.1111/j.1151-2916.1976.tb09451.x>
- 919
- 920
- 921 40. Chang H, Huang PJ, Hou SC (1999) Application of thermo-Raman spectroscopy to study dehydration of CaSO₄.2H₂O and CaSO₄.0.5H₂O. *Mater Chem Phys* 58(1):12–19
- 922
- 923
- 924
- 925 41. Black L, Breen C, Yarwood J et al (2006) Hydration of tricalcium aluminate (C3A) in the presence and absence of gypsum—studied by Raman spectroscopy and X-ray diffraction. *J Mater Chem* 16:1263. <https://doi.org/10.1039/b509904h>
- 926
- 927
- 928
- 929
- 930 42. Black L, Breen C, Yarwood J et al (2007) Structural features of C–S–H(I) and Its carbonation in air—a Raman spectroscopic study. Part II: carbonated phases. *J Am Ceram Soc* 90:908–917. <https://doi.org/10.1111/j.1551-2916.2006.01429.x>
- 931
- 932
- 933
- 934
- 935 43. Chollet M, Horgnies M (2011) Analyses of the surfaces of concrete by Raman and FT-IR spectroscopies: comparative study of hardened samples after demoulding and after organic post-treatment. *Surf Interface Anal* 43:714–725. <https://doi.org/10.1002/sia.3548>
- 936
- 937
- 938
- 939
- 940
44. Irassar EF, Bonavetti VL, González M (2003) Microstructural study of sulfate attack on ordinary and limestone Portland cements at ambient temperature. *Cem Concr Res* 33:31–41. [https://doi.org/10.1016/S0008-8846\(02\)00914-6](https://doi.org/10.1016/S0008-8846(02)00914-6)
- 941
- 942
- 943
- 944
- 945
45. Frost RL, Keeffe EC (2009) Raman spectroscopic study of the sulfite-bearing minerals scotlandite, hannebachite and orschallite: implications for the desulfation of soils. *J Raman Spectrosc* 40:244–248. <https://doi.org/10.1002/jrs.2089>
- 946
- 947
- 948
- 949
- 950
46. Scrivener KL, Crumbie AK, Laugesen P (2004) the interfacial transition zone (ITZ) between cement paste and aggregate in concrete. *Interface Sci* 12:411–421. <https://doi.org/10.1023/B:INTS.0000042339.92990.4c>
- 951
- 952
- 953
- 954
47. Mittermayr F, Rezvani M, Baldermann A et al (2015) Sulfate resistance of cement-reduced eco-friendly concretes. *Cement Concr Compos* 55:364–373. <https://doi.org/10.1016/j.cemconcomp.2014.09.020>
- 955
- 956
- 957
- 958
48. Appelo CAJ, Postma D (2004) *Geochemistry, groundwater and pollution*. CRC Press, Boca Raton
- 959
- 960
49. Grengg C, Gluth GJG, Mittermayr F et al (2021) Deterioration mechanism of alkali-activated materials in sulfuric acid and the influence of Cu: a micro-to-nano structural, elemental and stable isotopic multi-proxy study. *Cem Concr Res* 142:106373. <https://doi.org/10.1016/j.cemconres.2021.106373>
- 961
- 962
- 963
- 964
- 965
- 966
- 967
- Publisher's Note** Springer Nature remains neutral with regard to jurisdictional claims in published maps and institutional affiliations.
- 968
- 969
- 970
- 971
- Springer Nature or its licensor (e.g. a society or other partner) holds exclusive rights to this article under a publishing agreement with the author(s) or other rightsholder(s); author self-archiving of the accepted manuscript version of this article is solely governed by the terms of such publishing agreement and applicable law.
- 972
- 973
- 974
- 975
- 976
- 977
- 978
- 979
- 980



Journal:	11527
Article:	2346

Author Query Form

Please ensure you fill out your response to the queries raised below and return this form along with your corrections

Dear Author

During the process of typesetting your article, the following queries have arisen. Please check your typeset proof carefully against the queries listed below and mark the necessary changes either directly on the proof/online grid or in the 'Author's response' area provided below

Query	Details Required	Author's Response
AQ1	Please confirm if the author names are presented accurately and in the correct sequence (given name, middle name/initial, family name). Author 2 Given name: [Marielle Guéguen] Last name [Minerbe]. Also, kindly confirm the details in the metadata are correct.	
AQ2	Journal instruction requires a city for affiliations; however, these are missing in affiliation [1, 3]. Please verify if the provided city are correct and amend if necessary.	
AQ3	Please check and confirm the Figure 2 has changed to Figure 1, Figure3 has changed to Figure 2, Figure 1 has changed to Figure 3 are arranged in correct sequences.	
AQ4	Please check and confirm the inserted Table 2 is correctly identified.	
AQ5	Please check and confirm the Table 1 caption has changed to Table 2 is correctly identified.	